HEAL-T: AN EFFICIENT PPG-BASED HEART-RATE AND IBI ESTIMATION METHOD DURING PHYSICAL EXERCISE

Juan Manuel Mayor Torres, Arindam Ghosh, Evgeny A. Stepanov, Giuseppe Riccardi
Signals and Interactive Systems Lab
Department of Information Engineering and Computer Science
University of Trento, Trento, Italy
Email: {juan.mayortorres,arindam.ghosh,evgeny.stepanov,giuseppe.riccardi}@unitn.it

***Abstract*—Photoplethysmography (PPG) is a simple, unobtrusive and low-cost technique for measuring blood volume pulse (BVP) used in heart-rate (HR) estimation. However, PPG based heart-rate monitoring devices are often affected by motion artifacts in on-the-go scenarios, and can yield a noisy BVP signal reporting erroneous HR values. Recent studies have proposed spectral decomposition techniques (e.g. M-FOCUSS, Joint-Sparse-Spectrum) to reduce motion artifacts and increase HR estimation accuracy, but at the cost of high computational load. The singular-value-decomposition and recursive calculations present in these approaches are not feasible for the implementation in real-time continuous-monitoring scenarios. In this paper, we propose an efficient HR estimation method based on a combination of fast-ICA, RLS and BHW filter stages that avoids sparse signal reconstruction, while maintaining a high HR estimation accuracy. The proposed method outperforms the state-of-the-art systems on the publicly available TROIKA data set both in terms of HR estimation accuracy (absolute error of 2.25 $\pm$ 1.93 bpm) and computational load.**

1. Introduction

Accurate measurement of heart-rate (HR) is an important factor for several tasks such as early diagnosis of cardiovascular diseases, detection of stress and hypertension, and continuous monitoring of physical activities [1]. The recent advancements in photoplethysmography (PPG) have spurred the development of wearable wrist-based heart-rate sensors, which have gained wide acceptability due to an increased user comfort [2]. However, the blood volume pulse (BVP) reported by these PPG devices can often be highly contaminated by motion artifacts and noise; thus, either signal modeling or sparse signal reconstruction (SSR) are required to obtain a clean signal.

The current state-of-the-art on PPG signal reconstruction includes techniques such as adaptive filtering: Least Mean Squares (LMS) [2], [3], Recursive Least Squares (RLS) [4], Kalman and Wiener filters [5], and multiple Z-tap structures [6] that are commonly applied for online HR estimation due to their low computational load. However, they depend on a priori signal modeling and hence have a lower accuracy in the presence of motion artifacts. On the other hand, SSR techniques such as Focal-Underdetermined-System-Solver extension (M-FOCUSS) [7] and Multiple-Measured-Vectors (MMV) [8] generate a controlled level of spectrum sparsity for a sufficient spectral resolution and higher accuracy. However, this leads to higher computation load [9], [10].

In this paper, we propose a method for HR peak detection based on an initial moving-average-filter, an RLS scheme and an FIR Blackman-Harris-Window (BHW) filter's bandwidth variation. The proposed method is used to estimate HR values from spectral peaks and also to reconstruct the inter-beat interval (IBI) signal for each BVP signal window. The output signal is compared point-to-point against the reference electrocardiography (ECG) R-peak distance on TROIKA dataset. The computational efficiency of the proposed method (HEAL-T, henceforth) is compared in terms of the execution time to the LMS baseline and the M-FOCUSS method [7] of the TROIKA framework.

2. TROIKA Dataset

Publicly available TROIKA dataset [11] from the 2015 *IEEE Signal Processing Cup*[1] that closely mimics real-life motion activities is used throughout the experiments. The dataset consists of 5 minute treadmill trials by 12 different subjects. Each 5 min trial is divided into 6 different exercises as follows: 30 sec - rest (1-2 km/h), 1 min - Walking (6-8 km/h), 1 min - Running (10-12 km/h), 1 min - Walking (6-8 km/h), 1 min - Running (10-12 km/h) and finally 30 sec - rest (1-2 km/h). The provided signals are PPG, accelerometer and an ECG ground-truth. The sampling frequency for all the signals is $f_s = 125$ Hz. In TROIKA experiments on heart-rate estimation, the authors use a sliding window of 8 seconds with a 6 second overlap. The same settings are used throughout this paper.

3. Methodology

The HEAL-T pipeline (see Figure 1) consists of (a) initial filtering stage composed of a fast-ICA decomposition and a moving-average-filter application, (b) RLS filter scheme, (c) BHW bandwidth adjustment, (d) a spectral peak tracking process, and (e) an IBI estimation.

1. http://zhilinzhang.com/spcup2015/data.html

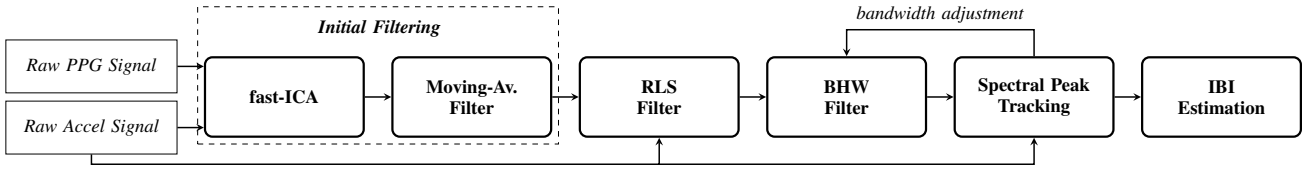

Figure 1: The pipeline of HEAL-T heart-rate estimation method that is applied per signal window.

3.1. Initial Filtering and Signal Modeling

In this stage the signal is filtered using statistical independence (e.g. ICA decomposition) and linear phase modeling (e.g. FIR schemes) per window to preserve BVP critical frequency ranges with an adequate spectral resolution.

3.1.1. fast-ICA. The fast-ICA algorithm is one of the fastest and efficient infomax algorithm implementations that ensures an adequate linear independence for low-frequency signal representations [12]. The fast-ICA decomposition (unmixing) models the negentropy gradient between PPG and Accelerometer channels to learn the unmixing matrix W_s [13]. The process returns 5 independent-components (ICs): one for each of the two PPG channels and one for each of the x, y and z axes of the Accelerometer signal. The subsequent mixing process integrates the two PPG channels (Accelerometer ICs are ignored).

3.1.2. Moving Average Filter. After the initial denoising and PPG harmonic reconstruction stages using fast-ICA, we apply moving average filter to ensure the removal of any residual motion artifacts. For each signal window X^i a compositional model is defined as $X^i = \text{PPG}^i + \text{Accel}^i + \text{N}^i$, where PPG^i and Accel^i are PPG and Accelerometer signals, respectively; and N^i is a high-frequency additive noise component. The filter is a computationally inexpensive convolution between X^i signal and a constant impulse response $1/M$ (Equation 1) that increases the SNR value and reduces the additive noise [14]. In order to fix the moving average filter's low-pass bandwidth below PPG channel frequency ranges $[0.9 - 2.5]$ Hz [15], the M value is set to 20.

$$\hat{X}^i(k) = \frac{1}{M} \sum_{n=0}^{M-1} X^i(k-n) \tag{1}$$

3.2. RLS Filter

To remove the incidence of motion artifacts in the PPG channels, we iteratively apply an RLS filter. RLS provides a non-misadjusted solution for least-squares cost function and a smooth spectral representation [16]. The filter is optimal adaptive noise-cancellation algorithm for low-frequency bands [2].

$$\omega(n) = \omega(n-1) - \kappa(n-1)\left[d(n) - \omega(n-1)\upsilon(n)\right] \tag{2}$$

$$P(n) = \lambda^{-1}P(n-1) - \lambda^{-1}\kappa(n-1)\upsilon^T(n)P(n-1) \tag{3}$$

$$\kappa(n) = \frac{\lambda^{-1}P(n-1)\upsilon(n)}{1 + \lambda^{-1}\upsilon^T(n)P(n-1)\upsilon(n)} \tag{4}$$

Equations 2 and 3 show the time-stepping of RLS, in which a forgetting factor λ modulates the filter weights $\omega(n)$ as a function of the previous ones $\omega(n-1)$. Other parameters, $\upsilon(n)$ (accelerometer signal), the factor $\kappa(n)$ (Equation 4), and the desired response $d(n) = \hat{X}^i(n)$ are synchronized in a sequence to generate an output $\hat{X}_r$. The RLS parameters are set as $\lambda = 0.99$ and $P(0) = 10^{-3}I$ [3], and the order of the filter is set as $N = 32$ [17].

3.3. BHW Filter

In this step, the signal $\hat{X}_r(k)$ (the output of RLS) is bound between $[0.9 - 2.5]$ Hz [15], reducing the phase nonlinearities and the stopband ripple [18]. A 4-term Blackman-Harris Window filter (Equation 5) is applied to achieve the desired stopband attenuation of $A_s = -60dB$. The BHW impulse response $\dot{h}(n)$ is truncated at $N = 150$, and a stop-band attenuation is achieved in $\hat{A}_s = -52.66dB$ with maximum stopband ripple of $|\delta_s| = 2.32dB$.[2] These values are sufficient for an accurate HR peak detection afterwards.

$$\dot{X}(k)^i = \sum_{n=0}^{N-1} \hat{X}_r(k-n)^i \dot{h}(n) \left[0.3587 - 0.4883cos\left(\frac{2\pi n}{N-1}\right) + 0.1413sin\left(\frac{4\pi n}{N-1}\right) - 0.0116cos\left(\frac{6\pi n}{N-1}\right)\right] \tag{5}$$

3.4. Spectral Peak Tracking

In [11] the authors demonstrate that even though SSR techniques increase the level of numerical sparsity, high amount of motion artifacts can increase the error in the HR peak detection process. The robustness of the peak detection can be improved by a *peak tracking* process [19]. Our implementation of the spectral peak tracking consists of three steps which run iteratively over each sliding window:

- HR Peak Selection
- HR Peak Verification
- BHW bandwidth Readjustment

3.4.1. HR Peak Selection. The peak selection process accepts PPG and Accelerometer signal streams as input and produces a set of HR candidate peaks as output. As a first step, this process generates a set of spectra from the PPG

2. When compared to other filters (e.g. Rectangular or Bartlett), BHW yields superior stopband attenuation and lower ripple variance.

and Accelerometer signals by running a fast Fourier transform (FFT) on these signal channels. Next, from the PPG spectrum, the *GetPeaks* function selects a set of frequencies which form a local maximum above 30% of the normalized spectrum amplitude. From this set, the first peak with a low accelerometer noise component is identified – this is done by selecting the peak for which the difference between the PPG PPG(n) and accelerometer spectrum amplitudes Accel(n) at the peak is greater than 0.10. Once this peak position is identified, the *SearchHrPeaks* function further selects a set of appropriate candidate peaks by searching either in the left or the right direction (given by the *searchDirection* flag) in the HR spectrum. The direction of the search may change in subsequent iterations based on the value of the *searchDirection* flag as is set in the peak verification stage.

Algorithm 1 HEAL-T HR Peak Selection Process

```
1: function PEAKSELECTION(PPG,ACCEL,NFFT,searchDirection)
2:     PPGSpec ← FFTfunc(PPG,NFFT)
3:     ACCELSpec ← FFTfunc(ACCEL,NFFT)
4:     peaks ← GetPeaks(HR)
5:     while n < count(peaks) do
6:         if |HR(n)| − |Accel(n)| > 0.10 then
7:             [HR] ← SearchHrPeak(HR,searchDirection)
8:             return [HR]
9:         else
10:            n ← n + 1
```

3.4.2. HR Peak Verification. From the set of candidate peaks returned by the peak selection process, the next step is to verify and select peaks which fall within a certain range. This range is given by range $=$ MeanPrevHR $\pm$ threshold, where *MeanPrevHR* is the mean heart rate values of the previous four windows and the *threshold* is set based on the variance of the candidate HR peaks in the current window. If the variance is below 0.10, then the *threshold* is set to 0.05, otherwise *threshold* is set to 0.10. The peak verification step iterates through the set of candidate HR peaks and determines if a peak lies within this range. Once we encounter a peak which is beyond this range, we readjust the BHW window and the *searchDirection* flag for peak search. If the HR peak value is below the range, the search direction for the next iteration is set to *left-to-right*; else it is set to *right-to-left*.

3.4.3. BHW bandwidth Readjustment. For the BHW bandwith readjustment, if the HR peak value is below the range determined in 3.4.2, the ω_p parameter of BHW window is increased by 0.30. Otherwise if the encountered HR peak value is above the range, then the ω_s value is decreased by 0.30. The default values of ω_p and ω_s are given by Equation 6.

$$[\omega_p, \omega_s] = \begin{cases} [0.9, 2.5] \text{ Hz}, & \text{if HR(1)} \leq 120 \text{ bpm} \\ [1.7, 3.5] \text{ Hz}, & \text{if HR(1)} > 120 \text{ bpm} \end{cases} \quad (6)$$

For the next iteration, we reapply the BHW window on the HR spectrum and redo the Peak Selection Stage. We perform this until the PeakSelection algorithm no longer returns any suitable candidate peak.

Algorithm 2 HEAL-T HR peak verification process

```
1: procedure PEAKVERIFICATION(PPG,ACCEL,NFFT = 65,536,Mean-
   PrevHR)
2:     [HR] ← PeakSelection(PPG,ACCEL,NFFT,searchDirection)
3:     HR_var ← Variance ([HR])
4:     if HR_var < 0.10 then
5:         threshold ← 0.05
6:     else
7:         threshold ← 0.10
8:     H̄R = MeanPrevHR
9:     n ← 1
10:    while HR(n) do
11:        if HR(n) ≤ H̄R − threshold ∗ H̄R then
12:            (HR(n), searchDirection) ← increase_peak(HR(n))
13:            Change_BHW(HR,ω_p + 0.30,ω_s)
14:        else if HR(n) ≥ H̄R + threshold ∗ H̄R then
15:            (HR(n), searchDirection) ← decrease_peak(HR(n))
16:            Change_BHW(HR,ω_p,ω_s − 0.30)
17:        else
18:            accept_peak(HR(n))
19:            n ← n + 1
```

3.5. IBI Estimation

The output of the previous step is converted to the time domain which yields a time-series of dichrotic notches. The selected notches are the ones with the amplitude above 50% for a given window. In the IBI estimation step we calculate the time-difference between the adjacent dichrotic notches. In order to estimate IBI for the whole signal, we need to compensate for the window overlaps. Thus, the IBIs between the notches in the overlap of the two consecutive windows are averaged, while maintaining the values from the non-overlapping segments. Finally, a smoothing spline (Cubic spline) is used to calculate the Interpolated-IBI (IIBI) and reduce undesired IBI spectral harmonics.

4. Evaluation and Results

In this section we evaluate HEAL-T in terms of the HR estimation accuracy and computational efficiency in comparison to the LMS baseline [17] (using the same paramenters) and the TROIKA framework (M-FOCUSS) [11].

4.1. HR Estimation Accuracy Evaluation

HR estimation performance is evaluated in two settings: (1) against the reference HR spectrum peaks, and (2) comparing the extracted IIBI (HR $= 60/$IIBI) to the reference ECG RR-peak distances (filtered using Daubechies Wavelet decomposition - level 3, order 3). Per subject and averaged performances for the first setting are reported in Tables 1 and 3 for train and test sets respectively; and for the second setting (IBI) in Table 2. Since ECG is not available for the test set, IBI-based evaluation is reported only only for the training set.

TABLE 1: Absolute error per subject on TROIKA training set for HEAL-T, LMS baseline [17] and the TROIKA framework [11]. The values significantly different for $p < 0.01$ are in bold italics.

Subjects	S1	S2	S3	S4	S5	S6	S7	S8	S9	S10	S11	S12	Avg	SD
HEAL-T	3.96	**1.73**	***0.91***	**2.21**	***0.32***	***1.19***	***0.32***	***0.47***	***0.26***	4.22	**0.87**	**1.41**	**1.49**	1.36
Han et al. [17]	5.21	2.22	1.45	3.44	0.88	3.42	0.58	1.33	2.45	4.55	1.21	4.33	2.59	1.57
Zhang et al. [11]	2.87	2.75	1.91	2.25	1.69	3.16	1.72	1.83	1.58	4.00	1.66	3.33	2.40	0.80

TABLE 2: IBI-based HR estimation on TROIKA training set for HEAL-T, LMS baseline [17] and the TROIKA framework [11]. The values significantly different for $p < 0.01$ are in bold italics.

Subjects	S1	S2	S3	S4	S5	S6	S7	S8	S9	S10	S11	S12	Avg	SD
HEAL-T	**5.42**	**4.54**	**2.53**	**3.39**	**2.55**	**3.04**	**2.26**	**2.58**	**2.75**	**5.04**	**3.46**	**3.21**	**3.40**	1.05
Han et al. [17]	6.41	5.64	6.01	5.43	2.88	4.12	4.08	3.45	3.88	6.46	5.55	5.75	4.97	1.22
Zhang et al. [11]	6.55	5.43	5.12	4.45	2.81	3.78	2.78	3.33	3.42	6.74	4.52	4.64	4.47	1.32

TABLE 3: Absolute errors per subject on TROIKA test set for HEAL-T, LMS baseline [17] and the TROIKA framework [11]. The values significantly different for $p < 0.01$ are in bold italics.

Subjects	S1	S2	S3	S4	S5	S6	S7	S8	Avg	SD
HEAL-T	**5.43**	**4.54**	**6.71**	**3.01**	**2.71**	**5.37**	**1.39**	**0.92**	**3.21**	2.10
Han et al. [17]	7.42	4.54	15.34	5.47	5.35	10.35	2.56	3.45	6.72	4.54
Zhang et al. [11]	5.78	4.33	12.45	3.79	3.09	7.74	4.56	2.42	5.47	3.53

For the HR-peak based evaluation we obtain the absolute error of 1.49 ± 1.36 bpm for the training (Table 1) and 3.21 ± 2.10 bpm for the test (Table 3) sets. The combined train-test set average absolute error is 2.25 ± 1.93 bpm (for comparison, for LMS and M-FOCUSS the combined averages are 4.08 ± 4.13 and 3.64 ± 2.59 bpm, respectively). For the IBI-based evaluation, we obtain the absolute error of 3.40 ± 1.05 bpm (Table 2).

Figures 2a and 2b illustrate the performances of the algorithm for subjects #9 (training set) and #7 (test set) against reference HR peaks. Figures 3a and 3b, on the other hand, present Bland-Altman plots for the two evaluation settings: for the HR-peak based setting we obtain Pearson $r = 0.9877$ and for the IBI-based setting – $r = 0.9813$.

4.2. Computational Efficiency Evaluation

Compared to the popular SSR techniques, the HEAL-T pipeline is less computationally demanding. For the preliminary evaluation of the computational load we use Matlab R2015a profiler to compute the execution time by varying the signal window size. The times reported in Figure 4 are averages of the 20 executions per window size [20]. The HEAL-T pipeline is compared to the LMS adaptive filtering (the baseline) and M-FOCUSS with the learning parameters set as $\lambda = 0.1$, $\gamma = 10^{-4}$ and $max\_iters = 500$ [7].

For comparison we have selected the subject #10 from the TROIKA dataset, as it represents the worst case scenario (in terms of the number of calls) for the HEAL-T. Window size is varied from 2 to 32 seconds with the 33% overlap. From the figure 4 we can observe that the HEAL-T execution time is 2 orders of magnitude lower that that of M-FOCUSS, and closer to the LMS baseline [21]. Thus, the HEAL-T approach can be considered more suitable for real-time HR monitoring.

5. Conclusion

We have presented an HR estimation pipeline that consists of fast-ICA, moving average filter, RLS, BHW and a spectral peak tracking process. In comparison to current systems, the HEAL-T pipeline is robust enough to accurately estimate HR in presence of high amount of motion artifacts. The approach is evaluated on the TROIKA dataset both in terms of the accuracy of HR estimation (averaging and IBI) and the computational efficiency. We have demonstrated that the proposed method outperforms the state of the art techniques on both criteria.

References

[1] J. Allen, "Photoplethysmography and its application in clinical physiological measurement," *Physiological measurement*, vol. 28, no. 3, p. R1, 2007.

[2] T. Shimazaki, S. Hara, H. Okuhata, H. Nakamura, and T. Kawabata, "Cancellation of motion artifact induced by exercise for ppg-based heart rate sensing," in *36th Annual International Conference of the IEEE Engineering in Medicine and Biology Society (EMBC)*. IEEE, 2014, pp. 3216–3219.

[3] T. Shimazaki and S. Hara, "Breathing motion artifact cancellation in ppg-based heart rate sensing," in *9th International Symposium on Medical Information and Communication Technology (ISMICT)*. IEEE, 2015, pp. 200–203.

[4] T. Schack, C. Sledz, M. Muma, and A. Zoubir, "A new method for heart rate monitoring during physical exercise using photoplethysmographic signals," *Eusipco 2015*, 2015.

[5] A. Temko, "Estimation of heart rate from photoplethysmography during physical exercise using wiener filtering and the phase vocoder," in *37th Annual International Conference of the Engineering in Medicine and Biology Society (EMBC)*. IEEE, 2015, pp. 1500–1503.

[6] J. M. M. Torres, "Eeg signals classification using linear and non-linear discriminant methods," *El Hombre y la Máquina*, no. 41, pp. 71–80, 2013.

[7] S. F. Cotter, B. D. Rao, K. Engan, and K. Kreutz-Delgado, "Sparse solutions to linear inverse problems with multiple measurement vectors," *IEEE Transactions on Signal Processing*, vol. 53, no. 7, pp. 2477–2488, 2005.

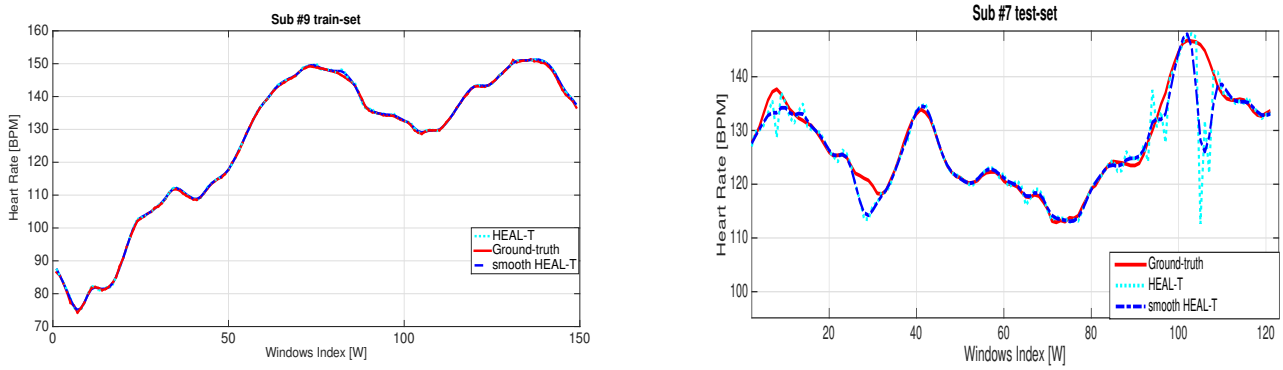

(a) (b)

Figure 2: HR estimation results for subjects #9 from the training set (2a) and #7 from the test set (2b), averaged for each 8 s window in trial.

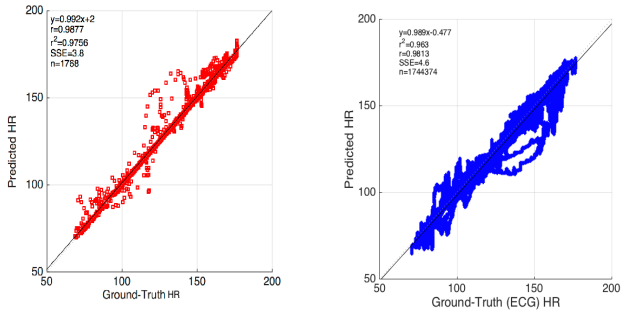

(a) (b)

Figure 3: Bland-Altman plots for HEAL-T HR estimation against reference HR-peaks (3a) and against reference ECG using IBI (3b).

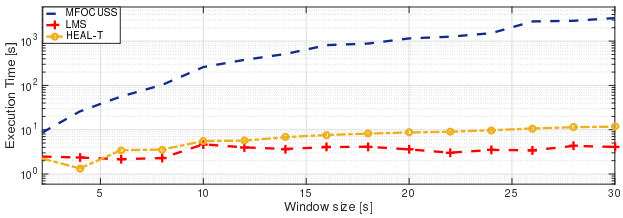

Figure 4: Comparison of HEAL-T to LMS [17] and M-FOCUSS [7], [11] in terms of execution time (log Y-axis) and the signal window size from 2 up to 32s (X-axis).

[8] Z. Zhang and B. D. Rao, "Sparse signal recovery with temporally correlated source vectors using sparse bayesian learning," *IEEE Journal of Selected Topics in Signal Processing*, vol. 5, no. 5, pp. 912–926, 2011.

[9] I. F. Gorodnitsky and B. D. Rao, "Sparse signal reconstruction from limited data using focuss: A re-weighted minimum norm algorithm," *IEEE Transactions on Signal Processing*, vol. 45, no. 3, pp. 600–616, 1997.

[10] L. Stankovic, S. Stankovic, and M. Amin, "Missing samples analysis in signals for applications to l-estimation and compressive sensing," *Signal Processing*, vol. 94, pp. 401–408, 2014.

[11] Z. Zhang, Z. Pi, and B. Liu, "Troika: A general framework for heart rate monitoring using wrist-type photoplethysmographic (ppg) signals during intensive physical exercise," *IEEE Transactions on Biomedical Engineering*, 2014.

[12] Y. Cui, C.-H. Fu, H. Hong, Y. Zhang, and F. Shu, "Non-contact time varying heart rate monitoring in exercise by video camera," in *International Conference on Wireless Communications & Signal Processing (WCSP)*. IEEE, 2015, pp. 1–5.

[13] A. Hyvärinen, "Fast and robust fixed-point algorithms for independent component analysis," *IEEE Transactions on Neural Networks*, vol. 10, no. 3, pp. 626–634, 1999.

[14] J. Lee, "Motion artifacts reduction from ppg using cyclic moving average filter." *Technology and health care: official journal of the European Society for Engineering and Medicine*, vol. 22, no. 3, pp. 409–417, 2014.

[15] M. K. Singh, A. Gupta, S. Permanand, U. Singh, O. Singh, Y. H. Kim, and A. K. Singh, "System modeling and signal processing of microwave doppler radar for cardiopulmonary sensing," in *International Conference on Signal Processing and Communication (ICSC)*. IEEE, 2015, pp. 227–232.

[16] P. C. Wei, J. Han, J. R. Zeidler, and W. H. Ku, "Comparative tracking performance of the lms and rls algorithms for chirped narrowband signal recovery," *IEEE Transactions on Signal Processing*, vol. 50, no. 7, pp. 1602–1609, 2002.

[17] H. Han and J. Kim, "Artifacts in wearable photoplethysmographs during daily life motions and their reduction with least mean square based active noise cancellation method," *Computers in biology and medicine*, vol. 42, no. 4, pp. 387–393, 2012.

[18] D. McDuff, S. Gontarek, and R. W. Picard, "Remote detection of photoplethysmographic systolic and diastolic peaks using a digital camera," *IEEE Transactions on Biomedical Engineering*, vol. 61, no. 12, pp. 2948–2954, 2014.

[19] B. Sun and Z. Zhang, "Photoplethysmography-based heart rate monitoring using asymmetric least squares spectrum subtraction and bayesian decision theory," *IEEE Sensors Journal*, vol. 15, no. 12, pp. 7161–7168, 2015.

[20] Y. M. Altman, *Accelerating MATLAB Performance: 1001 tips to speed up MATLAB programs*. CRC Press, 2014.

[21] A. D. Choudhury, A. Misra, A. Pal, R. Banerjee, A. Ghose, and A. Visvanathan, "Heartsense: Estimating heart rate from smartphone photoplethysmogram using adaptive filter and interpolation," in *Internet of Things. User-Centric IoT*. Springer, 2015, pp. 203–209.